

Center-of-mass quantization of excitons in CdTe/Cd_{1-x}Zn_xTe quantum wells

N. Tomassini and A. D'Andrea

Istituto Metodologie Avanzate Inorganiche, Consiglio Nazionale delle Ricerche, I-00016 Monterotondo Scalo, Roma, Italy

R. Del Sole

Dipartimento di Fisica, Università di Roma "Tor Vergata," via della Ricerca Scientifica 1, I-00173 Roma, Italy

H. Tuffigo-Ulmer and R. T. Cox

Departement de Recherche Fondamentale sur la Matière Condensée, Centre d'Etudes Nucleaires de Grenoble, 17 rue des Martyrs, F-38054 Grenoble Cedex 9, France

(Received 23 September 1994)

Photoluminescence excitation spectra are obtained for a large set of strained CdTe/Cd_{1-x}Zn_xTe single-quantum-well samples, as a function of well thickness. The experimental spectra are reproduced by an accurate variational exciton envelope function, expanded in products of electron and hole subbands. An analytical approximation for the exciton envelope function, well suited for thin films with finite confinement potentials, is also given. The good agreement obtained between theory and experiment for both methods strongly supports the concept of center-of-mass quantization for this quantum-well system in the thickness range from 180 to 1000 Å.

I. INTRODUCTION

Semiconductor quantum wells and superlattices are important and exciting model systems for investigating the physics and applications of quantum confinement. An impressive fabrication technology is available to make such structures. Only a few suitable combinations of materials (for instance, GaAs/Ga_{1-x}Al_xAs) are available for lattice-matched structures; it is now possible, however, to grow high-quality strained-layer structures which are thermodynamically stable below certain critical values of layer thicknesses.

Layered structures based on semiconductors of the family of II-VI compounds show strong excitonic effects and large optical nonlinearities. The recent observation of blue laser emission,¹ second-harmonic generation,² etc., points out the importance of a deeper fundamental knowledge of this important class of materials. Among II-VI systems, the CdTe/Cd_{1-x}Zn_xTe quantum-well system has been studied intensively due to its interesting fundamental properties such as, for example, a large value of the excitonic Rydberg and large strain splitting of the valence band, such that the lowest-energy transitions are spatially direct (type I) for heavy-hole excitons and spatially indirect (type II) for light-hole excitons.³⁻¹³ Because the Rydberg is quite large and the sequence of quantum states of the heavy-hole exciton is relatively unperturbed by light-hole excitonic states, these materials are well suited for providing clear experimental evidence of exciton center-of-mass quantization.⁸⁻¹³

Center-of-mass quantization means that, for an exciton confined by a potential well along the z direction (growth direction), the momentum of the center-of-mass along z , q_z , is quantized to discrete values characterized by a quantum number $n = 1, 2, 3, \dots$. In the simplest

description of this effect, applied to CdTe/Cd_{1-x}Zn_xTe quantum wells in Refs. 11-13, the relative motion of the electron and hole is totally unaffected by confinement. This description is qualitatively correct and remarkably useful for values of quantum-well width L_W down to about three times the exciton Bohr radius a_B . However, it cannot treat the progressive breakdown of the z -direction electron-hole correlation as L_W decreases to small values. Even at large L_W , the relative and center-of-mass motions can no longer be considered uncoupled in a transition layer of the order of a_B thick, at each surface of the well. At intermediate L_W , the two transition layers will interact,^{14,15} coupling the relative and the center-of-mass motions of the exciton in the whole well. Finally, at a very small well width, q_z is no longer a meaningful quantity. Instead, the conduction- and valence-band potential wells quantize the electron and hole momenta separately, giving a quasi-two-dimensional exciton characterized by two quantum numbers i and j , for electron and hole, respectively (this is the historically more familiar model, used extensively for III-V quantum-well systems; see Refs. 16 and 17).

The aim of the present paper is to test, for a large set of CdTe/Cd_{1-x}Zn_xTe single-quantum-well samples, two more sophisticated treatments of center-of-mass quantization, namely an analytical wave function that is correct in the range- L_W limit, and a variational expansion in terms of a large basis set of quasi-two-dimensional exciton wave functions that works well for small and moderate L_W values.

Clear-cut evidence for the concept of center-of-mass quantization of Wannier excitons was obtained by Cho *et al.*,¹⁸ discussing reflectance spectra of thick GaAs layers between Ga_{1-x}Al_xAs barriers obtained by Shultheis and Ploog.¹⁹ Further results for high-quality, thick

GaAs/Ga_{1-x}Al_xAs structures have been obtained by Kusano *et al.*²⁰ and by Tredicucci *et al.*²¹

In this paper, we present a systematic study of the optical response in single quantum wells of CdTe between Cd_{1-x}Zn_xTe barriers, as a function of the well thickness L_w in the range of moderate to large thicknesses: about 3–15 exciton Bohr radii (180–1000 Å). Because of lattice-mismatch problems, the Zn content x in the barrier alloy must be kept small. Section II describes the samples and shows some typical photoluminescence excitation (PLE) spectra. Section III presents two variational, envelope-function models, with different degrees of accuracy and complexity, for describing the exciton in quantum wells for finite-height barriers in this thickness range. Section IV is a comparison of the experimental and theoretical results, and Sec. V is the conclusion.

II. EXPERIMENT

The quantum-well structures discussed in this paper were grown in a Riber 32P molecular-beam epitaxy (MBE) facility, operated by a joint research group of the Commissariat à l'Énergie Atomique and the Centre National de la Recherche Scientifique in Grenoble. The substrates were (100)-oriented Cd_{1-x}Zn_xTe with $x=0.04$. The layers of CdTe and Cd_{1-x}Zn_xTe were deposited under excess Cd flux. Accurate control of layer thicknesses was achieved by monitoring oscillations of reflection high-energy electron diffraction (RHEED) during the growth.²² Two kinds of Cd_{1-x}Zn_xTe/CdTe/Cd_{1-x}Zn_xTe single-quantum-well structures were studied in the present work.

(a) Thirteen coherent structures: these were CdTe wells of thickness L_w ranging from 210 to 1000 Å, between 800-Å-thick Cd_{1-x}Zn_xTe barriers with $x=0.08$. These coherent structures are grown directly on the $x=0.04$ Cd_{1-x}Zn_xTe substrate and are constrained to its lattice parameter, the layer thicknesses being less than the critical values at which strain relaxation occurs. Since the lattice parameter decreases with increasing zinc content x , the CdTe well layer and the Cd_{1-x}Zn_xTe barrier layers have approximately equal but opposite strains, the CdTe being under biaxial compression and the Cd_{1-x}Zn_xTe under biaxial tension.

(b) Two buffered structures: these were CdTe wells between a 2–3- μ -thick buffer layer of Cd_{1-x}Zn_xTe with $x=0.12$ acting as the lower barrier, and an 800-Å top barrier of the same composition x . The thick buffer layer relaxes approximately to its free-standing lattice parameter, by formation of misfit dislocations at the buffer/substrate interface. Nearly all the misfit dislocations have grown out after 2–3- μ growth, so the structural quality is almost as good as that of the coherent samples (a). The CdTe well thickness was 405 Å for one of these samples, 180 Å for the other. A major advantage of these buffered structures in the present study is that substrate-related features in the photoluminescence excitation spectra are strongly attenuated by the presence of the thick buffer.

The optical measurements were done with the samples

mounted strain-free under pumped helium at 2 K. In the present paper we discuss photoluminescence excitation (PLE) spectra, obtained by monitoring luminescence below the lowest-energy free exciton emission as a function of the wavelength of an exciting laser (dye or Ti-sapphire Laser).

In Fig. 1, curves *a*, *c*, and *e* show emission spectra induced by light (blue light from an argon laser) of energy high up in the continuum states, for a coherent sample and the two buffered samples. The emission peak labeled *X* corresponds to recombination of the ground-state, heavy-hole exciton of the CdTe well. In the center-of-mass quantization description, it is the lowest quantized state $n=1$ of the $1s$ exciton. Alternatively, if the exciton is considered to be made of separately quantized electron (*E*) and heavy-hole (HH) subbands, it would be called the $1s E_1 HH_1$ exciton.

The emission peak labeled *Y* was initially thought to

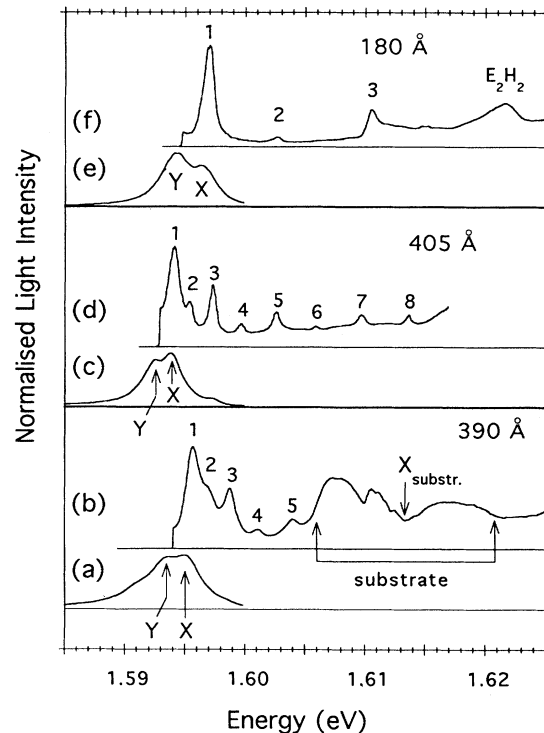


FIG. 1. Curves *a*, *c*, and *e* show photoluminescence (PL) spectra under blue laser light, and curves *b*, *d*, and *f* photoluminescence excitation spectra (PLE) for three CdTe/Cd_{1-x}Zn_xTe quantum-well samples ($L_w=390$, 405 , and 180 Å), respectively. The three emission spectra are normalized to the amplitude of their strongest peak, and the three PLE spectra to that of peak 1. Emission peaks *X* and *Y* correspond to the ground-state heavy-hole exciton and to negatively charged excitons (X^-), respectively. The PLE spectra are recorded by monitoring on peak *Y*, and show peaks corresponding to quantized exciton states $n=1, 2, 3, 4, \dots$. PL peak *X* corresponds to PLE peak $n=1$. The PLE of the “coherent” sample $L_w=390$ Å, grown directly on the Cd_{0.96}Zn_{0.04}Te substrate, shows substrate-exciton features. These are absent for the 405- and 180-Å samples, grown on thick Cd_{0.88}Zn_{0.12}Te buffers.

correspond to excitons trapped by some kind of defect or impurity, but has been reattributed recently to negatively charged excitons X^- ; that is, to excitons that have bound photoelectrons present metastably in the well.^{23,24} The transition corresponds to the recombination event $X^- \rightarrow e^- + \text{photon}$. In this paper, we are interested only in the free exciton line X and associated higher-energy transitions of the free exciton. PLE spectra showing the free-exciton states can be obtained conveniently by setting the monitoring monochromator on peak Y . Peak X is then included in the PLE spectrum.

The PLE spectra of the 15 samples all show a series of narrow peaks 1,2,3, . . . with progressively increasing spacing (see Fig. 1). Peak 1 coincides with emission peak X , except for a small Stokes shift. For the coherent samples, grown directly on the substrate, substrate-related features in the PLE limit the useful range of observation of the peaks; see Fig. 1, curve b . Absorption of light in the substrate, followed by excitation transfer back to the well, produces a broad double-hump structure, with a dip at the $1s$ exciton energy, in the PLE spectrum. This substrate response disappears almost entirely in the samples on a thick buffer layer; see Fig. 1, curves d and f .

In Fig. 1 (curve d), eight peaks can be counted (including X itself). For this thickness, ($L_w = 405 \text{ \AA}$, about six Bohr radii), the peaks correspond very well to quantized states $n = 1, 2, \dots, 8$ of the center-of-mass motion of the heavy-hole exciton.

As L_w decreases, the spacing of the peaks increases. In Fig. 1 (curve f), for $L_w = 180 \text{ \AA}$, three peaks remain. These three exciton states can be interpreted as center-of-mass quantized excitons $n = 1, 2, 3$. But at this well thickness, of the order of three Bohr radii, separate quantization of the electron and hole is an equally appropriate description. In the latter description, these excitons can be attached to pairs of subbands $E1H1$, $E1H2$, and $E1H3$, respectively: since $m_h \approx M (= m_h + m_e)$, the spacing of the hole subbands is similar to the spacing of the center-of-mass exciton levels.

The two descriptions correspond to the starting points for the two different theoretical approaches of Sec. III. Note also that the $E2H2$ exciton is now observable in Fig. 1 (curve f); this has no correspondence in the center-of-mass quantization description.

Intensity also arises from transitions involving the continuum of valence-band states that begins at the barrier level, and also from light-hole excitons. Because the CdTe valence band is split by strain, light-hole exciton states in the CdTe layer lie well above the heavy-hole exciton ground state: 12 and 36 meV higher in the coherent samples and in the more highly strained samples on relaxed buffers, respectively. Spatially indirect, type-II light-hole excitons exist at lower energy but have very low oscillator strengths for quantum wells with wide barriers (they have been studied in superlattices with thin barriers^{3,5}). This small involvement of light-hole excitons justifies the use of a two-band model.

PLE spectra of the series of 15 samples were compared with theoretically calculated absorption spectra obtained from the models of Sec. III. Comparisons of peak energies present no problem, but comparisons of peak intensi-

ties are valid only if the PLE gives a faithful representation of the true absorption. Ideally, when the quantum efficiency of the absorption and emission process is constant for all excitation wavelengths, PLE measures the sample's absorbance $A = (1 - r - t)/(1 - r)$, where t is the transmitted intensity and r the reflected intensity. That our PLE intensities are meaningful was supported by comparisons with intensities of corresponding features in reflectivity spectra.

III. THEORY

We consider a quantum well of thickness L_w grown along the z axis, ($-L_w/2 < Z < L_w/2$) and clad between two barriers of thickness L_B . In a two-band model and within the effective-mass approximation, the exciton Hamiltonian is

$$H = -\frac{\nabla_e^2}{2m_e} - \frac{\nabla_h^2}{2m_h} - \frac{1}{\epsilon_0 |\mathbf{r}_e - \mathbf{r}_h|} + V_e(z_e) + V_h(z_h), \quad (1)$$

where ϵ_0 is the bulk dielectric constant, and V_e and V_h are the confinement potentials for the electron and hole, respectively. We neglect image-potential effects, because we have nearly equal dielectric-constant values in the CdTe well and $\text{Cd}_{1-x}\text{Zn}_x\text{Te}$ barriers. In the following, we will consider two different variational models for the exciton.

A. Exciton envelope function expanded in e - h subbands

Here we place the physical system, namely the well clad with its two barriers, into a box of thickness $L_{\text{box}} = L_w + 2L_B$. For $L_{\text{box}} \rightarrow \infty$ we have discrete states localized in the well and a continuum of exciton states outside the well, while for large, but finite L_{BOX} value, we have a quasicontinuum of exciton states.

The eigenfunctions of the Hamiltonian (1) with azimuthal quantum number $m=0$, which are the only ones optically allowed, are obtained by a variational expansion in the following basis set of quasi-two-dimensional exciton functions:^{7,9}

$$\phi_{ij}(\rho, z_e, z_h) = N_{ij} c_i(z_e) v_j(z_h) \exp(-\alpha_{ij} r), \quad (2)$$

where $\mathbf{r} = \mathbf{r}_e - \mathbf{r}_h$ is the relative electron-hole coordinate, with $|\mathbf{r}| = \sqrt{\rho^2 + (z_e - z_h)^2}$, N_{ij} is the normalization constant of the function ϕ_{ij} , and $C_i(z_e)$ ($V_j(z_h)$) is the conduction (valence)-subband state of quantum number i (j). $C_i(z_e)$ is a subset of the orthonormalized eigenfunctions of the Hamiltonian,

$$\mathbf{H}_e = -\frac{1}{2m_e} \frac{\partial^2}{\partial z_e^2} + V_e(z_e). \quad (3)$$

Fulfilling the no-escape boundary conditions¹⁵ at the box edges:

$$c_i(z_e = \pm L_{\text{box}}/2) = 0 \quad \text{for } i = 1, 2, 3, \dots, \quad (4)$$

and the continuity conditions at the interfaces ($z_e = \pm L/2$). The hole subbands $V_j(z_h)$ are defined analogously. The radial variational parameters α_{ij} are

computed by minimizing the expectation value of the Hamiltonian (1) for each electron-hole wave function (2). The latter is meant to describe the lowest-energy exciton arising from the pair of subbands ij , in the absence of the interaction with other pairs of subbands. Higher exciton states are not included in the basis set, since they are less relevant for optical properties because of their smaller oscillator strengths.

The total exciton envelope function, which takes into account the interaction between excitons belonging to different subband pairs (ij), is

$$\Phi_n(\rho, z_e, z_h) = \sum_{ij} \beta_{ij,n} \phi_{ij}(\rho, z_e, z_h), \quad (5)$$

where $n=1,2,3,\dots,N$ labels the resulting exciton states. The exciton energies E_n and the expansion coefficients $\beta_{ij,n}$ are computed by diagonalizing the $N \times N$ matrix obtained by projecting the Hamiltonian (1) over the basis functions $\phi_{ij}(\rho, z_e, z_h)$. Binding energies with respect to the quantum-well band gap are computed as $E_{bn} = (E_e + E_h) - E_n$, where E_e (E_h) is the lowest electron (hole) eigenvalue of the one-electron Hamiltonian (3). The convergence of the higher levels in the well is tested by changing N ; ground convergence is obtained by retaining from 6 to 12 electron and hole subbands, namely for N from 36 to 144. Some inaccuracy may occur for higher-energy states, since we have included only the lowest-energy exciton (the 1s exciton) belonging to each subband pair.

The physical parameter values used in these calculations and those of Sec. III B are taken from Ref. 7, namely $m_h = 0.601$, $m_e = 0.087$, $E_{TO} = 1.595$ eV, and $\epsilon_0 = 9.7$. The heavy-exciton oscillator strength (needed for the calculation of optical properties) is $4\pi\beta = 0.006$, namely $\frac{3}{4}$ of the total oscillator strength determined from the bulk longitudinal-transverse splitting of 0.65 meV. Valence and conduction confinement potentials are chosen according to Ref. 5: $\Delta\varepsilon_v = 10$ meV and $\Delta\varepsilon_c = 40$ meV for all samples, except for the 180-Å sample, where the potentials adopted are $\Delta\varepsilon_v = 16$ meV and $\Delta\varepsilon_c = 67$ meV.

In Fig. 2 the exciton energy levels ($n=1-5$) are reported as a function of the well thickness. All subbands contribute to the exciton levels, demonstrating that we are in the range of weak confinement, where the center-of-mass quantization regime occurs. The lowest exciton state, however, shows some predominance of the lowest electron and hole subbands in the whole L_w range, decreasing as L_w increases, while no simple trend is apparent for the higher levels.

In Fig. 3 the lower exciton energies ($n=1-8$) for a sample of thickness $L_w = 405$ Å are shown as a function of n^2 . The trend is linear with two different slopes for low- and high- n^2 values. This is due to the fact that the hole may be outside the well for excitons with $n=7$ and 8. Although the exciton wave function is confined in the well, the confinement is weaker than for the lower-energy states, giving rise to the smaller slope in Fig. 3.

The wave-function expansion discussed here requires an increasing number of subbands as L_w increases, since the spacing of subbands decreases. The method becomes

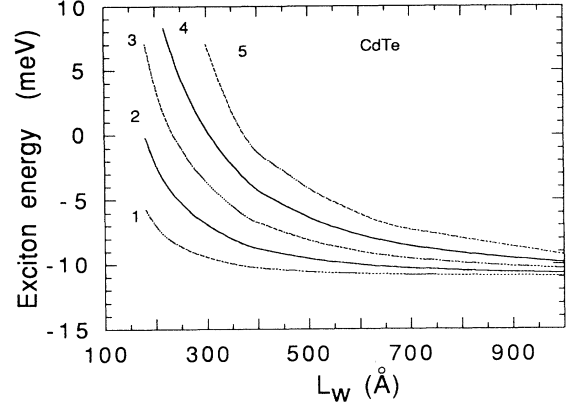


FIG. 2. Exciton energies computed according to the subband expansion model of Sec. III A as a function of well thickness for principal quantum number $n=1-6$. The values of the parameters are given in the text.

computationally inaccurate for L_w larger than 900 Å. Thicker slabs can be treated using the method described in Sec. III B (involving an adjustable parameter), which is also found to give good results for thicknesses down to near 200 Å.

B. Exciton analytic envelope-function model

It has been shown^{14,15} that for wide quantum wells excitons can be described within the effective-mass approximation by the envelope function:

$$\psi_n(\mathbf{r}, \mathbf{R}) = N_n Q_n(z, Z) \exp(-r/a_B), \quad (6)$$

where a_B is the exciton Bohr radius, $\mathbf{R} = (X, Y, Z)$ is the center-of-mass position, $\mathbf{r} = \mathbf{r}_e - \mathbf{r}_h$ is the relative electron-hole coordinate, and N_n is a normalization constant. The confinement function Q_n enforces the fulfillment of the no-escape boundary conditions in a unidimensional slab of width L_s , where the exciton is perfectly confined.

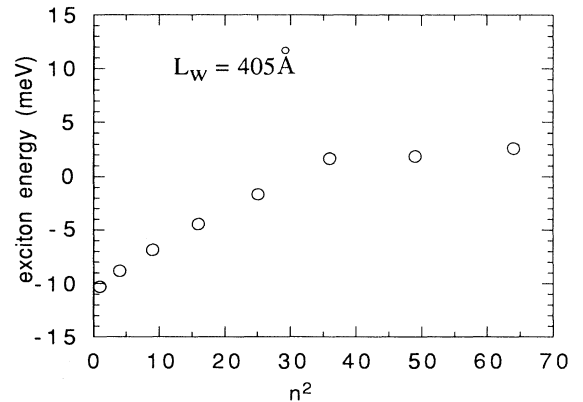


FIG. 3. Exciton energies computed according to the subband expansion model of Sec. III A for QW thickness $L_w = 405$ Å, as a function of n^2 . The values of the other parameters are given in the text.

If L_s is larger than three Bohr radii, and for excitons which are of even symmetry for reflection with respect to the central plane of the slab, the confinement function takes the form

$$Q_n(z, Z) = \cos(q_n Z) - F_e(z) \cosh(PZ) + F_0(z) \sinh(PZ), \quad (7)$$

where q_n for $n = 1, 3, 5, \dots$ is the exciton momentum along the Z axis, and P is a variational parameter obtained by minimizing the exciton energy. The inverse of the parameter P gives the depth over which the exciton vanishes at the surfaces of the slab. $F_e(z)$ and $F_0(z)$ are even and odd functions of z , respectively, determined by fulfilling the boundary conditions. For $z > 0$ these functions are

$$F_e(z) = [\sin(PZ_1) \cos(q_n Z_2) - \sinh(PZ_2) \cos(q_n Z_1)] / \sinh[P(Z_1 - Z_2)],$$

$$F_0(z) = [\cosh(PZ_1) \cos(q_n Z_2) - \cosh(PZ_2) \cos(q_n Z_1)] / \sinh[P(Z_1 - Z_2)],$$

where $Z_1 = L_s/2 - m_h z/M$ and $Z_2 = L_s/2 + m_e z/M$. The odd function $F_0(z)$ has a discontinuous derivative at $z=0$. Therefore the requirement of a continuous derivative of the total wave function (6) with respect to z , at $z=0$, is not obvious, and leads to the exciton quantization condition

$$q_n \tan(q_n L_s/2) + P \tanh(PL_s/2) = 0, \quad (8)$$

which determines the center-of-mass wave vector q_n . Analogous expressions are available for the odd exciton confinement functions $Q_n(z, Z)$, for $n = 2, 4, 6, \dots$.¹⁴

Note that the wave function (6) yields the correct limit for wide wells; at large L_w nonadiabatic terms coupling the kinetic energies of the center-of-mass and relative motions become small (see Fig. 9), and one then recovers the sum of the internal and center-of-mass energies:

$$E_n = -R^* + \frac{\hbar^2 \pi^2 n^2}{2M(L_s - 2/P)^2}, \quad (9)$$

where R^* is the effective Rydberg and M the total mass of the exciton. In order to arrive at (9), the asymptotic solution of (8) for large values of L_s has been used.

For infinitely high barriers, the slab thickness L_s is the actual thickness of the quantum well (QW), L_w . In the case of finite-height barriers, on the contrary, we can account for excitons spilling out from the interfaces by choosing L_s larger than the QW thickness. Since the inverse of P gives the depth over which the exciton wave function vanishes at the surfaces of the slab (the so-called transition or dead layer), the result is that the exciton is confined in an effective thickness L_{eff} defined by $L_{\text{eff}} = L_s - 2/P$. When L_{eff} turns out to be smaller than L_w ($L_{\text{eff}} < L_w$), the exciton is localized in the well, while for $L_{\text{eff}} > L_w$ it penetrates into the barriers.

L_s is the only adjustable parameter of the model, and its value is chosen in order to reproduce the energy dis-

tance between the first and second peaks of the experimental spectra ($E_{n=2} - E_{n=1}$). Moreover, for nominal QW thicknesses L_w ranging from 220 to 1000 Å in CdTe/Cd_{1-x}Zn_xTe samples, the value $\Delta = (L_s - L_w)/2$, which gives an estimate of the spilling out of the exciton wave functions at each interface, turns out to be roughly constant and about one effective Bohr radius (about 58 ± 14 Å).

The transition-layer depth $1/P$, computed using the parameter values of our CdTe/Cd_{1-x}Zn_xTe system quoted in Sec. III A, is plotted in Fig. 4 as a function of the well thickness for the lowest exciton state ($n=1$).

In Fig. 5 we show exciton energies and their adiabatic values [that is, according to Eq. (9)] as a function of n^2 calculated for the sample of thickness $L_w = 405$ Å. The higher-energy values show up a slight nonparabolicity as a function of the quantum number n . This is due to the deviation of the solutions of Eq. (8) from their large- L_s behavior. Such nonparabolicity is weaker than that predicted by the subband expansion calculation described in Sec. III A and shown in Fig. 3. The model of Sec. III A describes the higher exciton states ($n=7$ and 8) as having a much weaker confinement in the well (due to the delocalization of the hole) and this gives the large nonparabolicity of Fig. 3. In the analytical envelope-function model of the present section, states $n=7$ and 8 do not have a qualitatively different nature from the lower-energy states, and this analytical model gives, in fact, a better fit to experiment for these states.

C. Optical response of excitons in quantum wells

In order to calculate the optical properties, we solve Maxwell's equations for light normally incident on an unsupported QW. A detailed description of the method of solution, which fully accounts for spatial dispersion, is given in Ref. 15 within the framework of the analytical envelope-function method described in Sec. III B. The procedure is similar in the case of the subband expansion method of Sec. III A: the main ingredient of the calculation, that is the exciton wave function at zero electron-hole separation, is obtained in this case from Eq. (5), tak-

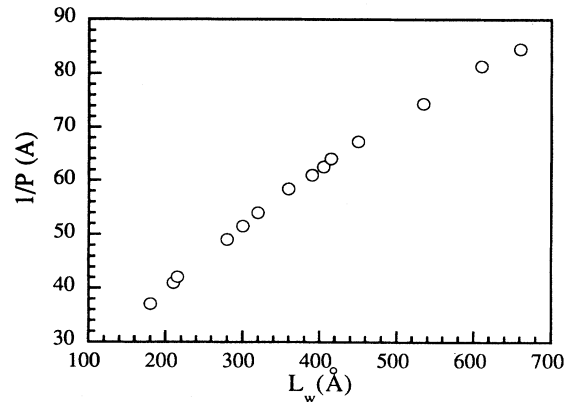


FIG. 4. Transition-layer depth $1/P$ of the analytical envelope-function model of Sec. III B as a function of the QW thickness. The values of the parameters are given in the text.

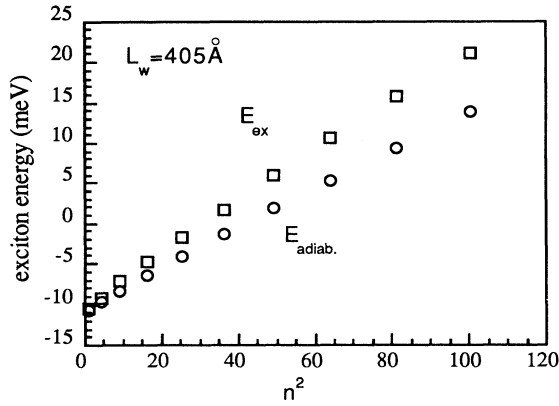


FIG. 5. Exciton energies computed according to the analytical envelope-function model of Sec. III B and their adiabatic approximation [Eq. (9)] as a function of the well thickness. The values of the parameters are given in the text.

ing $\rho=0$ and $z_e=z_h$.

Finally, we calculate the absorbance $A=(1-r-t)/(1-r)$ in terms of the reflectivity r and the transitivity t .

IV. DISCUSSION

We first compare the experimental PLE spectra with absorption spectra computed by the subband expansion of Sec. III A. The parameters adopted for the calculation are kept constant for all samples of the set. In the calculation, the barrier thickness is chosen large enough not to influence the exciton eigenvalues for states confined in the well; this value is smaller ($L_B=400$ Å) than the actual values of L_B in the samples ($L_B=800$ Å).

In Fig. 6 we compare calculated and experimental values for the energy differences between the lowest exciton state ($n=1$) and the higher states ($n=2,3,4,5$) for the different samples as a function of the inverse squared well thickness. We plot energy differences here rather than absolute values because the absolute energy of the experimental exciton spectrum shifts rigidly up or down with changes in strain state resulting from different substrate or buffer compositions for the different samples.

As a first approximation, the experimental peak positions vary linearly with $1/L_w^2$, but there is a definite downward deviation from straight-line plots. The theoretical energies computed with the model of Sec. III A are in very good agreement with the experimental points. They reproduce the deviations from a $1/L_w^2$ dependence very well. Note that they reproduce higher excited states ($n=6$) that are very sensitive to the values adopted for the confinement potentials.

In Fig. 7 we compare experimental and theoretical spectra for three quantum wells of nominal thicknesses 660, 405, and 180 Å, respectively [Figs. 7(a), 7(b), and 7(c)]. The calculation was carried out according to the subband expansion of Sec. III A. As already noted (Fig. 6), the theory compares well with experimental spectra as concerns the positions of the lower-energy exciton peaks, while for the higher exciton states it is impossible to

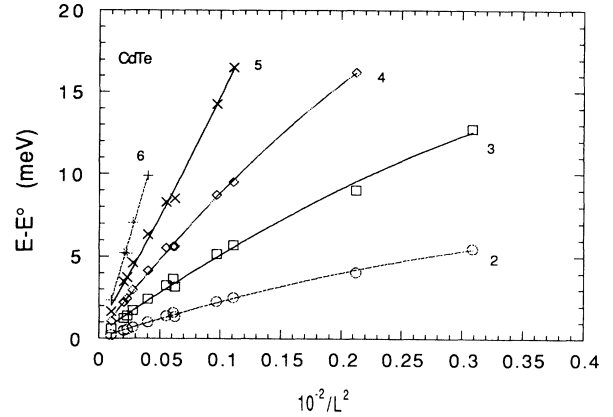


FIG. 6. Exciton energies computed according to the subband expansion model of Sec. III A as a function of the well thickness for different values of the principal quantum number $n=1-6$ (solid curves). The symbols are the corresponding peak positions extracted from the experimental data.

reproduce the experimental line shape because the model does not embody light-hole excitons and the higher-energy electron-hole continuum resulting from the motion in the (x,y) plane.

The calculations of the optical absorption correctly reproduce the alternations in intensity between odd- n and even- n states, but for the larger well widths they do not fall off as rapidly with n as the experimental peaks do. The reason for this may be the transformation of exciton states into polariton states as L_w becomes comparable to the light wavelength in the medium, $\lambda=2600$ Å (see Ref. 18 for a detailed discussion).

We emphasize that this model does not embody adjustable parameters and correctly reproduces exciton states confined in the wells; moreover, results of the same quality, not shown in the present paper, are obtained for the other samples.

Next, the same set of physical parameters used in the former calculation will be adopted for reproducing the experimental spectra by the analytical exciton envelope function of Sec. III B. The Δ value is taken constant (see Sec. III B) for all samples. Moreover, if we take E_T as an adjustable parameter in order to take into account the different strain states of the samples, its value is found to be almost constant ($E_T=1.5945$ eV) for the whole set of samples, except for the $L_w=405$ Å buffered sample, where $E_T=1.5934$ eV.

In Fig. 8 we compare theory and experiment for three samples with thicknesses of 660, 405, and 220 Å [see, respectively, Figs. 8(a), 8(b), and 8(c)]; we cannot reproduce the 180-Å sample very well because its thickness is at the limit of validity of the model (about three Bohr radii¹⁵). The agreement between theory and experiment is good for this model, at least as concerns the energies of the exciton peaks. In fact, for the 405-Å sample [see Fig. 8(b)] this model shows a better agreement than that obtained for the former model [Fig. 7(b)]; in particular the higher-energy states $n=7$ and 8 are reproduced in a better way. This is strong evidence that the heavy-hole exciton is also

strongly localized in the well for the $n=7$ and 8 states, and that the weaker localization predicted by the sub-band expansion model of Sec. III A might be an artifact of using a slightly inaccurate value of the valence-band offset.

In Fig. 9 we compare the energies of the lowest exciton state computed by the models of Secs. III A and III B and in the adiabatic limit [Eq. (9)] for all values of L_w . While

the energies given by the two models show the same trend as a function of quantum-well thicknesses from three to ten Bohr radii, the energies computed by Eq. (9) recover the correct energy values only for thicknesses greater than six Bohr radii. This can be considered, for the lowest exciton state, a lower bound of well thickness for the validity of the extreme model of the center-of-

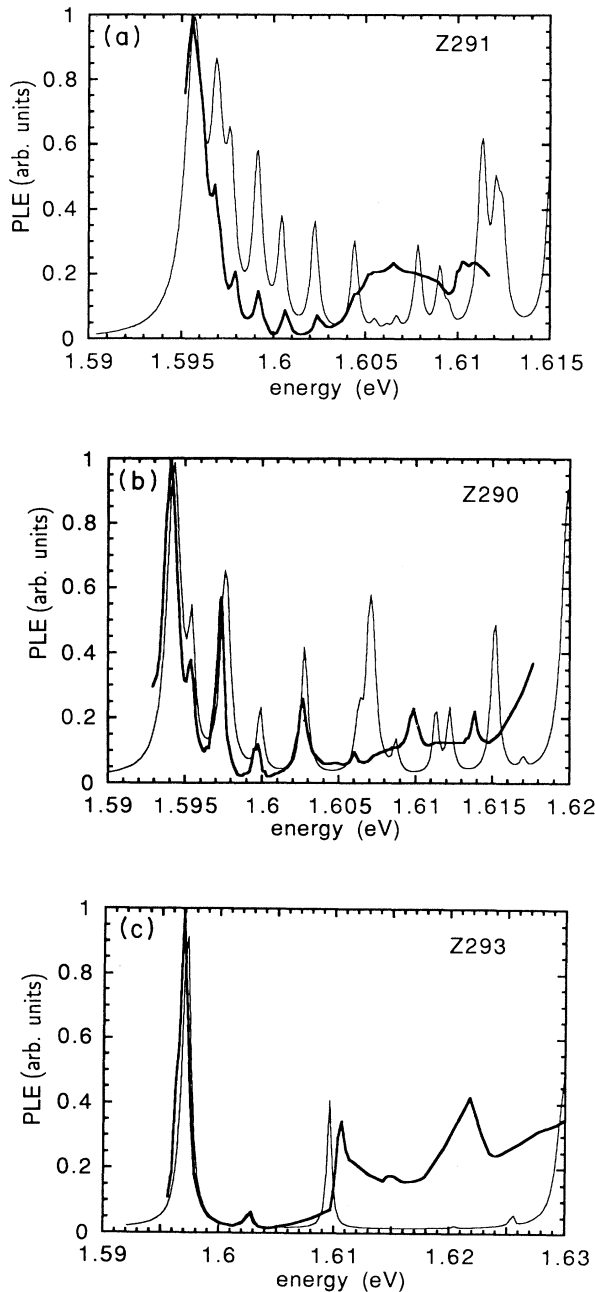


FIG. 7. Experimental PLE spectra (heavy lines) and absorption calculated according to the model of Sec. III A (lighter lines) for the samples: Z291, of nominal thickness $L_w=660$ Å (a); Z290, of nominal thickness $L_w=405$ Å (b); and Z293, of nominal thickness $L_w=180$ Å (c). The values of the parameters are given in the text.

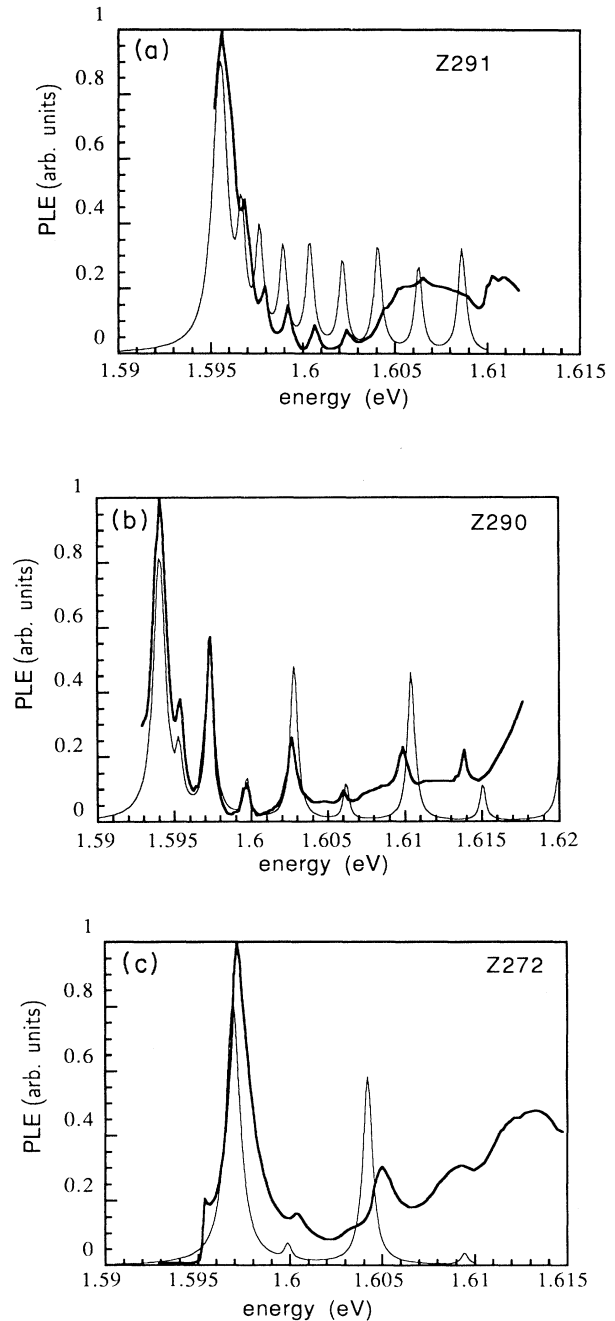


FIG. 8. Experimental PLE spectra and absorption calculated according to the model of Sec. III B for the samples: Z291, of nominal thickness $L_w=660$ Å (a); Z290, of nominal thickness $L_w=405$ Å (b); and Z272, of nominal thickness $L_w=220$ Å (c). The values of the parameters are given in the text.

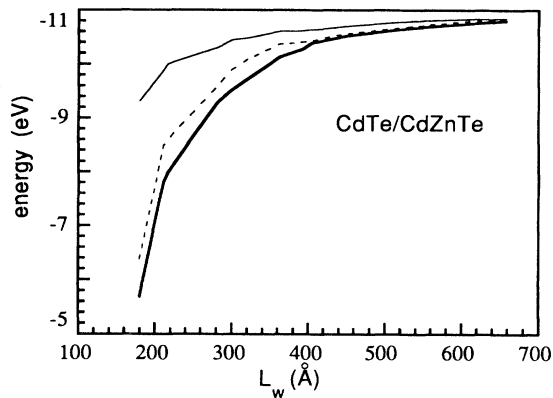


FIG. 9. Lowest exciton energies as a function of the well thickness computed according to the subband expansion model of Sec. III A (solid line), the analytical envelope function model of Sec. III B (dashed line), and the adiabatic approximation given by Eq. (9) (thin solid line).

mass quantization decoupled from the internal motion, confirming the Altarelli-Platero calculations.⁹

V. CONCLUSIONS

A large number of photoluminescence excitation spectra obtained for CdTe/Cd_{1-x}Zn_xTe quantum-well structures was interpreted by using an accurate exciton model (Sec. III A) that reproduces not only the lowest exciton

state, but also the higher ones up to the limit of the barrier continuum. Theory compares well with experimentally measured positions of exciton peaks for excitons confined in the well.

The above method becomes numerically inaccurate for quantum wells wider than 900 Å. An alternative method, a simple analytical model for the exciton envelope function which is well suited to reproduce experimental data for samples with finite-height barriers and large quantum-well thicknesses, down to $L_w > 3a_B$, was presented (Sec. III B) and compared with experiment.

This systematic study of the lowest exciton energies ($n=1$) in samples of thicknesses ranging from 180 to 1000 Å has demonstrated that the Wannier exciton follows the simple center-of-mass quantization of Eq. (9) for well thicknesses greater than six Bohr radii. For thicknesses from six to three Bohr radii, although the coupling between relative and center-of-mass motions is not negligible, center-of-mass quantization is still approximately valid. The nonparabolicity of the exciton energies as a function of the principal quantum number n was discussed and compared with experimental data.

ACKNOWLEDGMENTS

The samples studied in this work were grown by G. Lentz, N. Magnea, and H. Mariette. Two of us (A.D.A. and R.D.S.) acknowledge partial support of the European Community within the program ESPRIT, Basic Research, Action No. 6878, EASI.

- ¹J. Ding, H. Jeon, T. Ishiara, M. Hagerott, A. V. Nurmikko, H. Luo, N. Samarth, and J. Furdyna, *Phys. Rev. Lett.* **69**, 1707 (1992).
- ²F. Minami, K. Inoue, Y. Kato, K. Yoshida, and E. Era, *Phys. Rev. Lett.* **67**, 3708 (1991).
- ³H. Tuffigo, N. Magnea, H. Mariette, A. Wasiela, and Y. Merle d'Aubigne', *Phys. Rev. B* **43**, 14 629 (1991).
- ⁴E. Deleporte, J. M. Berroir, C. Delalande, N. Magnea, H. Mariette, J. Allegre, and J. Calatayud, *Phys. Rev. B* **45**, 6305 (1992).
- ⁵P. Peyla, Y. Merle d'Aubigne', A. Wasiela, R. Romestain, H. Mariette, M. D. Sturge, N. Magnea, and H. Tuffigo, *Phys. Rev. B* **46**, 1557 (1992).
- ⁶N. T. Pelekanos, H. Haas, N. Magnea, H. Mariette, and A. Wasiela, *Appl. Phys. Lett.* **61**, 3154 (1992).
- ⁷A. D'Andrea and N. Tomassini, *Phys. Rev. B* **47**, 7176 (1993).
- ⁸H. Tuffigo, in *Proceedings of "Optics of Excitons in Confined Systems"*, edited by A. D'Andrea, R. Del Sole, R. Girlanda, and A. Quattropani (Institute of Physics, Bristol, 1992), p. 37.
- ⁹G. Platero and M. Altarelli, in *Proceedings of the 20th International Conference on the Physics of Semiconductors*, edited by E. M. Anastassakis and J. D. Joannopoulos (World Scientific, Singapore, 1990), p. 1489.
- ¹⁰A. D'Andrea, R. Del Sole, H. Tuffigo, and R. T. Cox, in *Proceedings of the 20th International Conference on the Physics of Semiconductors* (Ref. 9), p. 1497.
- ¹¹Y. Merle d'Aubigne', Le Si Dang, A. Wasiela, N. Magnea, F. Dal'bo, and A. Millon, *J. Phys. (Paris) Colloq.* **48**, C5-4310 (1988).
- ¹²H. Tuffigo, R. T. Cox, N. Magnea, Y. Merle d'Aubigne', and A. Million, *Phys. Rev. B* **37**, 4310 (1988).
- ¹³H. Tuffigo, R. T. Cox, G. Lentz, N. Magnea, and H. Mariette, *J. Cryst. Growth* **101**, 778 (1990).
- ¹⁴A. D'Andrea, R. Del Sole, and K. Cho, *Europhys. Lett.* **11**, 169 (1990).
- ¹⁵A. D'Andrea and R. Del Sole, *Phys. Rev. B* **41**, 1413 (1990).
- ¹⁶R. Dingle, W. Wiegmann, and C. H. Henry, *Phys. Rev. Lett.* **33**, 827 (1974).
- ¹⁷G. Bastard, E. E. Mendez, L. L. Chang, and L. Esaki, *Phys. Rev. B* **26**, 1974 (1982).
- ¹⁸K. Cho, A. D'Andrea, R. Del Sole, and H. Ishihara, *J. Phys. Soc. Jpn.* **59**, 1853 (1990).
- ¹⁹L. Shultheis and K. Ploog, *Phys. Rev. B* **29**, 7058 (1984).
- ²⁰J. Kusano, Y. Segawa, M. Mihara, Y. Aoyagi, and S. Namba, *Solid State Commun.* **72**, (1989); J. Kusano, G. E. W. Bauer, and Y. Aoyagi, *J. Appl. Phys.* **75**, 289 (1994).
- ²¹A. Tredicucci, Y. Chen, F. Bassani, J. Massies, C. Deparis, and G. Neu, *Phys. Rev. B* **47**, 10 348 (1993).
- ²²G. Lentz, A. Ponchet, N. Magnea, and H. Mariette, *Appl. Phys. Lett.* **55**, 2733 (1989).
- ²³K. Kheng, R. T. Cox, Y. Merle d'Aubigne', F. Bassani, K. Saminadayar, and S. Tararenko, *Phys. Rev. Lett.* **71**, 1752 (1993).
- ²⁴K. Kheng *et al.*, *Surf. Sci.* **305**, 225 (1994).